Article

Slow Translation of a Composite Sphere in an Eccentric Spherical Cavity

Yi C. Chen and Huan J. Keh *

Department of Chemical Engineering, National Taiwan University, Taipei 10617, Taiwan; r12524072@ntu.edu.tw
* Correspondence: huan@ntu.edu.tw; Tel.: +886-2-33663048

Abstract: This semi-analytical study is presented examining the quasi-steady creeping flow caused by a soft (composite) spherical particle, which is a hard (impermeable) sphere core covered by a porous (permeable) layer, translating in an incompressible Newtonian fluid within a non-concentric spherical cavity along the line joining their centers. To solve the Brinkman and Stokes equations for the flow fields inside and outside the porous layer, respectively, general solutions are constructed in two spherical coordinate systems attached to the particle and cavity individually. The boundary conditions at the cavity wall and particle surface are fulfilled through a collocation method. Numerical results of the normalized drag force exerted by the fluid on the particle are obtained for numerous values of the ratios of core-to-particle radii, particle-to-cavity radii, the distance between the centers to the radius difference of the particle and cavity, and the particle radius to porous layer permeation length. For the translation of a soft sphere within a concentric cavity or near a small-curvature cavity wall, our drag results agree with solutions available in the literature. The cavity effect on the drag force of a translating soft sphere is monotonically increasing functions of the ratios of core-to-particle radii and the particle radius to porous layer permeation length. While the drag force generally rises with an increase in the ratio of particle-to-cavity radii, a weak minimum (surprisingly, smaller than that for an unconfined soft sphere) may occur for the case of low ratios of core-to-particle radii and of the particle radius to permeation length. This drag force generally increases with an increase in the eccentricity of the particle position, but in the case of low ratios of core-to-particle radii and particle radius to permeation length, the drag force may decrease slightly with increasing eccentricity.

Keywords: creeping flow; soft sphere; hydrodynamic drag force; boundary effect; spherical cavity

1. Introduction

The motions of solid particles in viscous fluids at small Reynolds numbers continue to receive plentiful attention from investigators in the fields of chemical, biomedical, civil, mechanical, and environmental engineering. This creeping motion is fundamental in nature, but permits us to develop rational thoughts of various practical systems and industrial processes such as sedimentation, filtration, agglomeration, electrophoresis, microfluidics, aerosol technology, rheology of suspensions, and motions of cells in blood vessels. The theoretical investigation of this topic grew out of the classic work of Stokes [1] on the motion of a hard (impermeable) sphere in an unbounded Newtonian fluid, and was extended to the creeping motion of a composite sphere [2].

A soft sphere of radius b is a composite particle with a hard sphere core of radius a covered by a porous (permeable) layer of uniform thickness $b - a$. In the limiting cases of $a = b$ and $a = 0$, the soft sphere degenerates to a hard sphere and a porous sphere, respectively, of radius b. A biological cell with protein surface attachments [3] and a polystyrene latex with a macromolecular surface layer [4] are examples of a soft particle. To achieve the steric stabilization of colloid suspensions, polymers are deliberately adsorbed onto hard particles to form permeable layers [5].

In practical cases of creeping motion, the particles are not isolated, and the ambient fluid is bounded by solid walls. Therefore, it is important to determine if the existence of adjacent boundaries affects the motion of the particles significantly. The low-Reynolds-number motions of a hard sphere confined by boundaries, such as those within a concentric or nonconcentric spherical cavity [6–9], near one or two large planes [10–15], and in a circular cylinder [16–18], were analyzed extensively. Some fluid streamline plots showing the recirculation flow for the case of a spherical particle within the concentric spherical cavity were presented [6]. Similarly, the creeping motions of a soft sphere inside a concentric spherical cavity [19–22], near one or two large planes [4,23] and in a circular cylinder [24], were theoretically investigated. Although the motions of an entirely porous sphere [25–27] within an eccentric spherical cavity were examined, the translation of a general soft particle inside a non-concentric cavity has not been studied yet.

The system of a soft sphere translating within a spherical cavity can be viewed as an idealized model for the capture of composite particles in a filter composed of connecting spherical pores. The hydrodynamic interaction between the soft particle and the cavity wall determines the deposition behavior of particles toward confining walls and the capture efficiency of filters. The objective of this article is to obtain a theoretical solution for the quasi-steady slow translation of a soft spherical particle in a non-concentric spherical cavity along their common diameter. A boundary collocation method [7] will be used to solve the creeping flow equations applicable to this system, and the wall-corrected hydrodynamic drag exerted on the particle will be obtained in many cases. The drag results reveal some interesting features of the influence of the cavity wall on soft particle motion. Although the drag force generally increases with increasing the particle-to-cavity radius ratio, a weak minimum (even less than that for an unconfined soft particle) may occur at low ratios of core-to-particle radii and of the particle radius to permeation length. This drag force generally increases with increasing eccentricity of the particle position, but for low values of these ratios, the drag force may decrease slightly with increasing eccentricity.

2. Analysis

As shown in Figure 1, we consider the quasi-steady flow caused by a soft spherical particle of radius b translating with a velocity U in an incompressible Newtonian fluid inside an eccentric spherical cavity of radius c along their common diameter (z axis). Here, (ρ, ϕ, z) and (r_2, θ_2, φ) represent the circular cylindrical and spherical coordinate systems, respectively, with their origins attached to the cavity center. The soft particle has a hard core of radius a and a porous layer of thickness $b - a$. The center of the particle is situated at a distance d from the cavity center instantaneously. The purpose of this is to determine the correction for the hydrodynamic drag experienced by the particle because of the existence of the cavity.
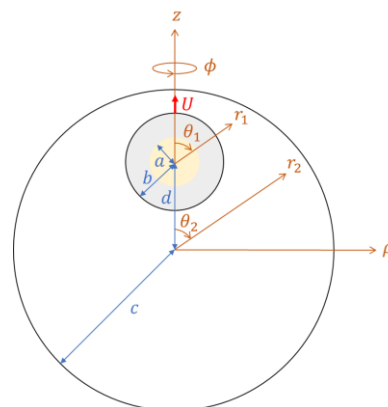

Figure 1. A soft spherical particle translating inside a spherical cavity along their common diameter.

Owing to the low Reynolds number (Re < 0.1), the fluid motion is governed by the Brinkman (inside the porous surface layer) and Stokes (outside the soft sphere) equations for the axisymmetric creeping flow,

$$(E^2 - \lambda^2)E^2\hat{\Psi} = 0 \quad (a \leq r_1 \leq b), \tag{1}$$

$$E^2(E^2\Psi) = 0 \quad (r_1 \geq b \text{ and } r_2 \leq c), \tag{2}$$

where (r_1, θ_1, ϕ) is the spherical coordinate system based on the center of the soft particle, λ^{-1} is the permeation length or square root of the fluid permeability in the porous layer, $\hat{\Psi}$ and Ψ are stream functions of the flow in the porous layer and external flow, respectively, related to their nontrivial velocity components $(\hat{v}_{r_i}, \hat{v}_{\theta_i})$ and (v_{r_i}, v_{θ_i}) in spherical coordinates by

$$(\hat{v}_{r_i}, v_{r_i}) = -\frac{1}{r_i^2 \sin\theta_i} \frac{\partial(\hat{\Psi}, \Psi)}{\partial\theta_i}, \ (\hat{v}_{\theta_i}, v_{\theta_i}) = \frac{1}{r_i \sin\theta_i} \frac{\partial(\hat{\Psi}, \Psi)}{\partial r_i}, \tag{3}$$

the Stokes operator

$$E^2 = \frac{\partial^2}{\partial r_i^2} + \frac{\sin\theta_i}{r_i^2} \frac{\partial}{\partial\theta_i}\left(\frac{1}{\sin\theta_i} \frac{\partial}{\partial\theta_i}\right), \tag{4}$$

and $i = 1$ or 2.

The boundary conditions for the fluid flow are

$$r_1 = a: \ \hat{v}_{r_1} = \hat{v}_{\theta_1} = 0, \tag{5}$$

$$r_1 = b: \ v_{r_1} = \hat{v}_{r_1}, \ v_{\theta_1} = \hat{v}_{\theta_1}, \tag{6a}$$

$$\tau_{r_1\theta_1} = \hat{\tau}_{r_1\theta_1}, \ \tau_{r_1 r_1} - p = \hat{\tau}_{r_1 r_1} - \hat{p}, \tag{6b}$$

$$r_2 = c: \ v_{r_2} = -U\cos\theta_2, \ v_{\theta_2} = U\sin\theta_2. \tag{7}$$

Here, $(\hat{\tau}_{r_1\theta_1}, \hat{\tau}_{r_1 r_1})$ and $(\tau_{r_1\theta_1}, \tau_{r_1 r_1})$ are the nontrivial stress components in the spherical coordinates (r_1, θ_1, ϕ) for the flow in the porous surface layer and external flow, respectively, $\hat{p}$ and p are the matching pressure profiles, and Equations (5)–(7) take a reference frame translating with the soft particle. For axisymmetric motions with the effective viscosity of the fluid in the porous layer equal to the bulk fluid viscosity [2,28] and satisfying Equation (6a) simultaneously, the boundary condition (6b) is equivalent to [29]

$$r_1 = b: \ \frac{\partial v_{\theta_1}}{\partial r_1} = \frac{\partial \hat{v}_{\theta_1}}{\partial r_1}, \ p = \hat{p} \ (\text{or } \tau_{r_1 r_1} = \hat{\tau}_{r_1 r_1}). \tag{8}$$

The various boundary conditions to describe flow characteristics at the boundary between a porous medium and a free fluid have received considerable attention in the literature [28,30]. Although a jump in shear stress was suggested to be accounted for in Equation (6b) [31], the present case of zero jump can be physically realistic and mathematically consistent [2].

We can express the stream functions as [7,23]

$$\hat{\Psi} = \sum_{n=2}^{\infty} \left\{ A_{1n}r_1^n + B_{1n}r_1^{-n+1} + [C_{1n}I_{n-1/2}(\lambda r_1) + D_{1n}K_{n-1/2}(\lambda r_1)](\lambda r_1)^{1/2} \right\} G_n^{-1/2}(\cos\theta_1), \tag{9}$$

$$\Psi = \sum_{n=2}^{\infty} [(A_{2n}r_2^n + C_{2n}r_2^{n+2})G_n^{-1/2}(\cos\theta_2) + (B_{2n}r_1^{-n+1} + D_{2n}r_1^{-n+3})G_n^{-1/2}(\cos\theta_1)], \tag{10}$$

where I_n and K_n are the modified Bessel functions of the first and second kinds of order n, respectively, and $G_n^{-1/2}$ is the Gegenbauer polynomial of the first kind of order n and degree $-1/2$. The unknown coefficients A_{in}, B_{in}, C_{in}, and D_{in} ($i = 1$ or 2) will be determined using Equations (5)–(7). When constructing the solution (10), the general solutions of

Equation (2) in the two spherical coordinate systems can be superimposed due to the linearity of this equation.

Application of Equation (3) to Equations (9) and (10) leads to the components of fluid velocities, $(\hat{v}_\rho, \hat{v}_z)$ and (v_ρ, v_z) for the flow inside the porous layer and external flow, respectively, in circular cylindrical coordinates as

$$\hat{v}_\rho = \sum_{n=2}^{\infty} \left[A_{1n} A_n'(r_1, \theta_1) + B_{1n} B_n'(r_1, \theta_1) + C_{1n} \gamma_n'(r_1, \theta_1) + D_{1n} \delta_n'(r_1, \theta_1) \right], \tag{11a}$$

$$\hat{v}_z = \sum_{n=2}^{\infty} \left[A_{1n} A_n''(r_1, \theta_1) + B_{1n} B_n''(r_1, \theta_1) + C_{1n} \gamma_n''(r_1, \theta_1) + D_{1n} \delta_n''(r_1, \theta_1) \right], \tag{11b}$$

$$v_\rho = \sum_{n=2}^{\infty} \left[A_{2n} A_n'(r_2, \theta_2) + C_{2n} C_n'(r_2, \theta_2) + B_{2n} B_n'(r_1, \theta_1) + D_{2n} D_n'(r_1, \theta_1) \right], \tag{12a}$$

$$v_z = \sum_{n=2}^{\infty} \left[A_{2n} A_n''(r_2, \theta_2) + C_{2n} C_n''(r_2, \theta_2) + B_{2n} B_n''(r_1, \theta_1) + D_{2n} D_n''(r_1, \theta_1) \right], \tag{12b}$$

where A_n', A_n'', B_n', B_n'', C_n', C_n'', D_n', D_n'', γ_n', γ_n'', δ_n', and δ_n'' are functions of spherical coordinates (r, θ) defined by Equations (A1)–(A12) in Appendix A. Applying boundary conditions (5)–(7) to Equations (11) and (12), we obtain

$$\sum_{n=2}^{\infty} \left[A_{1n} A_n'(a, \theta_1) + B_{1n} B_n'(a, \theta_1) + C_{1n} \gamma_n'(a, \theta_1) + D_{1n} \delta_n'(a, \theta_1) \right] = 0, \tag{13a}$$

$$\sum_{n=2}^{\infty} \left[A_{1n} A_n''(a, \theta_1) + B_{1n} B_n''(a, \theta_1) + C_{1n} \gamma_n''(a, \theta_1) + D_{1n} \delta_n''(a, \theta_1) \right] = 0, \tag{13b}$$

$$\sum_{n=2}^{\infty} \left\{ \left[A_{2n} A_n'(r_2, \theta_2) + C_{2n} C_n'(r_2, \theta_2) \right]_{r_1 = b} + B_{2n} B_n'(b, \theta_1) + D_{2n} D_n'(b, \theta_1) \right.$$
$$\left. - A_{1n} A_n'(b, \theta_1) - B_{1n} B_n'(b, \theta_1) - C_{1n} \gamma_n'(b, \theta_1) - D_{1n} \delta_n'(b, \theta_1) \right\} = 0, \tag{14a}$$

$$\sum_{n=2}^{\infty} \left\{ \left[A_{2n} A_n''(r_2, \theta_2) + C_{2n} C_n''(r_2, \theta_2) \right]_{r_1 = b} + B_{2n} B_n''(b, \theta_1) + D_{2n} D_n''(b, \theta_1) \right.$$
$$\left. - A_{1n} A_n''(b, \theta_1) - B_{1n} B_n''(b, \theta_1) - C_{1n} \gamma_n''(b, \theta_1) - D_{1n} \delta_n''(b, \theta_1) \right\} = 0, \tag{14b}$$

$$\sum_{n=2}^{\infty} \left\{ \left[A_{2n} A_n^*(r_2, \theta_2) + C_{2n} C_n^*(r_2, \theta_2) \right]_{r_1 = b} + B_{2n} B_n^*(b, \theta_1) + D_{2n} D_n^*(b, \theta_1) \right.$$
$$\left. - A_{1n} A_n^*(b, \theta_1) - B_{1n} B_n^*(b, \theta_1) - C_{1n} \gamma_n^*(b, \theta_1) - D_{1n} \delta_n^*(b, \theta_1) \right\} = 0, \tag{14c}$$

$$\sum_{n=2}^{\infty} \left\{ \left[A_{2n} A_{2n}^{**}(r_2, \theta_2) + C_{2n} C_n^{**}(r_2, \theta_2) \right]_{r_1 = b} + B_{2n} B_{2n}^{**}(b, \theta_1) + D_{2n} D_n^{**}(b, \theta_1) \right.$$
$$\left. - A_{1n} A_{1n}^{**}(b, \theta_1) - B_{1n} B_{1n}^{**}(b, \theta_1) - C_{1n} \gamma_n^{**}(b, \theta_1) - D_{1n} \delta_n^{**}(b, \theta_1) \right\} = 0, \tag{14d}$$

$$\sum_{n=2}^{\infty} \left\{ A_{2n} A_n^{***}(c, \theta_2) + C_{2n} C_n^{***}(c, \theta_2) + \left[B_{2n} B_n^{***}(r_1, \theta_1) + D_{2n} D_n^{***}(r_1, \theta_1) \right]_{r_2 = c} \right\} = -U, \tag{15a}$$

$$\sum_{n=2}^{\infty} \left\{ A_{2n} A_n^{****}(c, \theta_2) + C_{2n} C_n^{****}(c, \theta_2) + \left[B_{2n} B_n^{****}(r_1, \theta_1) + D_{2n} D_n^{****}(r_1, \theta_1) \right]_{r_2 = c} \right\} = -U, \tag{15b}$$

where A_n^*, A_{1n}^{**}, A_{2n}^{**}, A_n^{***}, A_n^{****}, B_n^*, B_{1n}^{**}, B_{2n}^{**}, B_n^{***}, B_n^{****}, C_n^*, C_n^{**}, C_n^{***}, C_n^{****}, D_n^*, D_n^{**}, D_n^{***}, D_n^{****}, γ_n^*, γ_n^{**}, δ_n^*, and δ_n^{**} are functions of (r, θ) defined by Equations (A13)–(A34).

Equations (10), (12), (14), and (15) can be expressed in a single spherical coordinate system by using the following transformation formulas between (r_2, θ_2) and (r_1, θ_1):

$$r_2 = \left[(r_1 \cos\theta_1 + d)^2 + r_1^2(1 - \cos^2\theta_1)\right]^{1/2}, \tag{16a}$$

$$\cos\theta_2 = (d + r_1 \cos\theta_1)/r_2. \tag{16b}$$

The subscripts 1 and 2 of the coordinates r and θ in the previous equations can be interchanged through the sign conversion of d.

To exactly satisfy the conditions in Equations (13)–(15), solutions of the whole infinite unknown constants A_{in}, B_{in}, C_{in}, and D_{in} are required. But, the collocation technique [7] enforces boundary conditions at a limited number of discrete points on the longitudinal semicircle of each of the spherical surfaces (from $\theta_i = 0$ to $\theta_i = \pi$ at $r_1 = a$, $r_1 = b$, and $r_2 = c$) and truncates the infinite series in Equations (9)–(12) to finite series. If the longitudinal semicircle is approximated by N discrete points satisfying the conditions in Equations (5)–(7), then the infinite series in Equations (9)–(12) are truncated after N terms, resulting in $8N$ linear algebraic equations in the truncated form of Equations (13)–(15). These equations can be solved numerically to produce the $8N$ unknowns A_{in}, B_{in}, C_{in}, and D_{in} required for the truncated Equations (9)–(12). Once these unknowns are solved for a sufficiently large number of N, the fluid velocity can be fully obtained. Details of the boundary collocation scheme are given in a previous paper on the translational motion of a hard spherical particle in a cavity [7].

The drag force exerted by the external fluid on the soft particle (in the opposite direction of U) can be determined from [7]

$$F = 4\pi\eta D_{22}, \tag{17}$$

where η is the viscosity of the fluid. The previous equation indicates that only the lowest-order constant D_{22} contributes to the hydrodynamic force acting on the particle. If the soft sphere is located at the center of the spherical cavity ($d = 0$), D_{22} can be obtained analytically as Equation (A35).

When the porous layer of the soft particle vanishes, it reduces to a hard particle of radius $a = b$, Equations (1), (5), (6b), (8), (9), (11), (13), and (14c,d) are trivial, $\hat{v}_\rho = \hat{v}_z = 0$, $A_{1n} = B_{1n} = C_{1n} = D_{1n} = 0$, and Equations (14a,b) and (15) only are needed to be solved for the $4N$ unknown constants A_{2n}, B_{2n}, C_{2n}, and D_{2n}. When the hard core disappears ($a = 0$), the soft sphere reduces to a porous particle of radius b, Equations (5) and (13) are trivial, $B_{1n} = D_{1n} = 0$, and Equations (14) and (15) only are needed for the $6N$ unknowns A_{1n}, C_{1n}, A_{2n}, B_{2n}, C_{2n}, and D_{2n}.

In the limiting case of $b/c = 0$, the soft sphere is unconfined, and Equation (17) can be expressed analytically as [2,19]

$$\begin{aligned}F_0 &= -6\pi\eta\lambda^{-1}U\{W\lambda a\cosh\lambda a - 3\lambda^2 a^2(V + \lambda a\sinh\lambda a) + \cosh(\lambda b - \lambda a)[W(\lambda aV - \lambda b\cosh\lambda a) \\ &+ 3\lambda^3 a^2 b\sinh\lambda a] + \sinh(\lambda b - \lambda a)[W\cosh\lambda a + 3\lambda^2 a^2(\lambda aV - \sinh\lambda a)]\}\{(\lambda a\sinh\lambda b \\ &- \cosh\lambda a)[(W + 3\lambda b)\cosh(\lambda b - \lambda a) + 3(\lambda^2 a^2 - 1)\sinh(\lambda b - \lambda a) - 6\lambda a]\}^{-1}\end{aligned} \tag{18}$$

where

$$V = \lambda b\sinh\lambda b - \cosh\lambda b, \tag{19a}$$

$$W = 2\lambda^3 b^3 + \lambda^3 a^3 + 3\lambda a. \tag{19b}$$

For the cases of $a = b$ and $a = 0$, Equation (18) becomes Stokes' law ($F_0 = 6\pi\eta bU$) for a hard sphere and the corresponding result for a porous sphere, respectively. In the limits $\lambda b \to \infty$ (impermeable in the porous surface layer of the particle) and $\lambda b = 0$ (completely permeable in the porous surface layer), Equation (18) again simplifies to Stokes' law for hard spheres of radii b and a, respectively.

3. Results and Discussion

Results of the hydrodynamic drag force acting on a soft sphere translating inside an eccentric spherical cavity, obtained with good convergence by using the boundary collocation technique described in the previous section for various values of the ratios of the core-to-particle radii a/b, particle-to-cavity radii b/c, distance between the centers to radius difference of the cavity and particle $d/(c-b)$, and particle radius to porous layer permeation length λb, are presented for cases of porous sphere ($a = 0$) and general soft sphere in Tables 1 and 2, respectively. The drag force F_0 acting on an identical particle in the unbounded fluid given by Equation (18) is used to normalize the cavity-corrected value F. These results converge to at least the significant digits as given in the tables, and agree with the available analytical solution in the concentric limit $d/(c-b) = 0$ given in Appendix B. Also, our results in the limit $b/c \to 0$ (vanishing cavity wall curvature compared with the particle) but finite in $b/(c-d)$ are in agreement with the results for a soft spherical particle translating perpendicular to a large plane wall obtained by Chen and Ye [23]. In the limit $\lambda b \to \infty$ (or $a = b$), our results agree with those [7] obtained for a hard sphere translating in a corresponding cavity. $F/F_0 = 1$ as $b/(c-d) = 0$ (the cavity wall is far away from the particle) as expected, irrespective of the other parameters.

Table 1. The normalized drag force F/F_0 experienced by a porous sphere ($a = 0$) translating inside a spherical cavity at different values of $d/(c-b)$, b/c, and λb.

$d/(c-b)$	b/c	F/F_0				
		$\lambda b = 0.1$	$\lambda b = 1$	$\lambda b = 10$	$\lambda b = 100$	$\lambda b = 500$
0.25	0.1	0.9949	1.0380	1.2619	1.3015	1.3048
	0.2	0.9702	1.0569	1.6570	1.7931	1.8046
	0.3	0.9626	1.0890	2.2845	2.6428	2.6738
	0.4	0.9673	1.1303	3.3190	4.2244	4.3053
	0.5	0.9766	1.1728	5.0786	7.4727	7.6958
	0.6	0.9869	1.2108	8.0957	15.1128	15.8189
	0.7	0.9953	1.2397	12.9569	37.0789	39.9815
	0.8	1.0004	1.2572	19.2043	1.244×10^2	1.447×10^2
	0.9	1.0023	1.2643	23.9350	6.971×10^2	1.195×10^3
	0.95	1.0018	1.2652	24.8577	1.692×10^3	7.847×10^3
	0.975	1.0023	1.2649	24.9698	2.025×10^3	2.702×10^4
	0.99	1.0026	1.2654	25.0226	2.212×10^3	4.747×10^4
	0.999	1.0027	1.2655	25.0247	2.245×10^3	5.564×10^4
0.5	0.1	0.9901	1.0419	1.3253	1.3778	1.3821
	0.2	0.9389	1.0379	1.8007	1.9933	2.0100
	0.3	0.8681	1.0007	2.5106	3.0559	3.1058
	0.4	0.8634	1.0237	3.6576	5.0423	5.1760
	0.5	0.9022	1.0925	5.5773	9.1351	9.5057
	0.6	0.9435	1.1622	8.7466	18.7607	19.9314
	0.7	0.9755	1.2169	13.5844	46.2215	51.0323
	0.8	0.9943	1.2500	19.4783	1.521×10^2	1.857×10^2
	0.9	1.0014	1.2631	23.9276	7.604×10^2	1.522×10^3
	0.95	1.0023	1.2649	24.8262	1.600×10^3	9.517×10^3
	0.975	1.0010	1.2633	24.8767	1.756×10^3	1.958×10^4
	0.99	1.0021	1.2647	24.9957	2.147×10^3	3.790×10^4
	0.999	1.0027	1.2654	25.0246	2.245×10^3	5.564×10^4

The normalized drag force F/F_0 of a porous sphere ($a = 0$) translating axisymmetrically within a non-concentric spherical cavity is plotted against the parameters b/c, $d/(c-b)$, and λb in Figures 2–4, respectively. For fixed values of $d/(c-b)$ and b/c, the normalized force F/F_0 increases monotonically with a decrease in permeability or an increase in λb from unity (with $F = F_0 = 0$) at $\lambda b = 0$ to a finite value (or infinity at the limit $b/c = 1$ where the particle seals the cavity and $d = 0$) as $\lambda b \to \infty$, as illustrated in Table 1 and Figures 2a, 3b, and 4a,b. F/F_0 changes weakly with $d/(c-b)$ and b/c (less than 27%

for all cases with $b/c \leq 0.999$) as $\lambda b \leq 1$. When b/c and $d/(c-b)$ are not close to unity, the normalized force F/F_0 on a porous particle with $\lambda b > 100$ approaches that when $\lambda b \to \infty$ (a porous sphere of little permeability performs as a hard sphere), but when the porous sphere is near the wall, the difference in F/F_0 can become significant.

Table 2. The normalized drag force F/F_0 experienced by a soft sphere with $\lambda b = 1$ translating inside a spherical cavity at different values of $d/(c-b)$, b/c, and a/b.

$d/(c-b)$	b/c	F/F_0		
		$a/b = 0.5$	$a/b = 0.8$	$a/b = 0.95$
0.25	0.1	1.1387	1.2304	1.2858
	0.2	1.2976	1.5592	1.7389
	0.3	1.5105	2.0622	2.5003
	0.4	1.7973	2.8642	3.8672
	0.5	2.1822	4.2100	6.5427
	0.6	2.7002	6.6206	12.4338
	0.7	3.3984	11.3193	27.8263
	0.8	4.3408	21.5831	80.8279
	0.9	5.6261	48.0522	3.924×10^2
	0.95	6.4505	78.1032	1.327×10^3
	0.975	6.9168	1.021×10^2	2.846×10^3
	0.99	7.2290	1.224×10^2	5.793×10^3
	0.999	7.4251	1.369×10^2	9.589×10^3
0.5	0.1	1.1668	1.2842	1.3569
	0.2	1.3269	1.6664	1.9150
	0.3	1.4769	2.1951	2.8323
	0.4	1.7280	3.0461	4.4755
	0.5	2.1288	4.5028	7.6832
	0.6	2.6887	7.1133	14.6867
	0.7	3.4357	12.1532	32.7173
	0.8	4.4057	22.8894	93.2114
	0.9	5.6672	49.4743	4.310×10^2
	0.95	6.4648	78.8504	1.351×10^3
	0.975	6.9173	1.009×10^2	2.153×10^3
	0.99	7.2224	1.221×10^2	5.328×10^3
	0.999	7.4251	1.369×10^2	9.587×10^3

For given values of λb and $d/(c-b)$, as illustrated in Table 1 and Figures 2a,b, 3a, and 4b, the normalized force F/F_0 acting on a porous sphere generally is an increasing function of the ratio of the particle-to-cavity radii b/c from unity at $b/c = 0$ to a finite value (or infinity if $\lambda b \to \infty$) at $b/c = 1$. This is because the closer the cavity wall is to the particle surface, the stronger the hydrodynamic hindrance effect of the cavity wall. Unexpectedly, when $d/(c-b)$ is not near zero (the particle eccentricity within the cavity is not negligible) and λb is smaller than about two (the porous sphere is relatively permeable), F/F_0 may not be a monotonic function of b/c, and will reach a minimum either greater or less than unity at medium values of b/c. That is, the existence of a confinement wall can decrease the hydrodynamic force on a porous sphere, and this counter-intuitive behavior seems to be caused by the approximations in the porous particle where the volume-averaged superficial velocity of the local fluid is used, and its effective viscosity is equal to the bulk fluid viscosity [28]. The dependence of F/F_0 on b/c disappears at the limit $\lambda b = 0$, but is strong when λb is large.

For specified values of b/c and λb, the normalized force F/F_0 generally increases with the increasing eccentricity parameter $d/(c-b)$ from one finite value in the concentric situation $d/(c-b) = 0$ to another value at the contact limit of the particle and cavity surfaces $d/(c-b) = 1$, as shown in Table 1 and Figures 2b, 3a,b, and 4a. These results indicate that the hydrodynamic hindrance of particle motion due to the proximity of the cavity wall is enhanced on the proximal side and reduced on the distal side of the particle,

with an enhanced net effect. But, when the value of λb is small (say, less than about 3) or b/c is large (say, greater than about 0.8, as indicated in Figure 3a), F/F_0 may decrease slightly (even to less than unity) as $d/(c-b)$ increases. This behavior seems to be also caused by the approximations in the porous particle where the volume-averaged superficial velocity of the local fluid is used. The variation of F/F_0 with $d/(c-b)$ vanishes at the limits $\lambda b = 0$ and $b/c = 0$, but is obvious when the value of λb is large.

(**a**)　　　　　　　　　　　　　　　　(**b**)
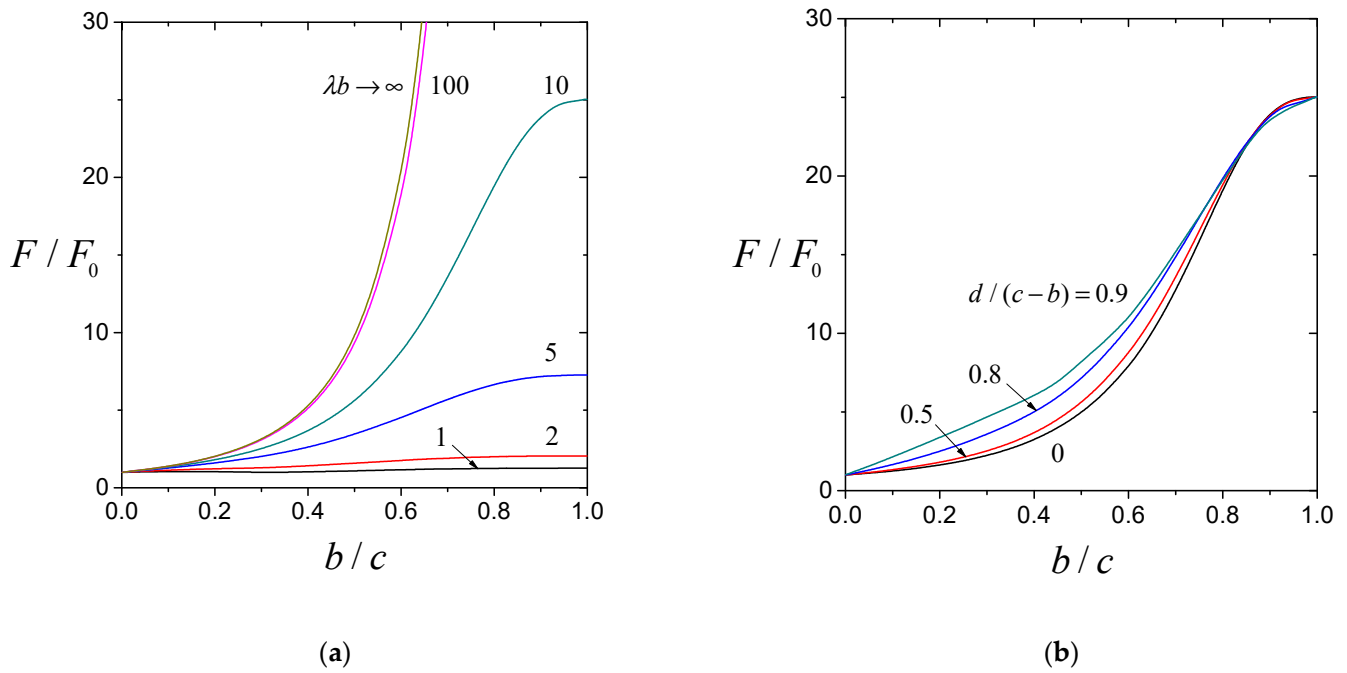
Figure 2. Normalized drag force F/F_0 of a porous sphere ($a = 0$) translating inside a spherical cavity versus the ratio of particle-to-cavity radii b/c: (**a**) $d/(c-b) = 1/2$ and (**b**) $\lambda b = 10$.

(**a**)　　　　　　　　　　　　　　　　(**b**)
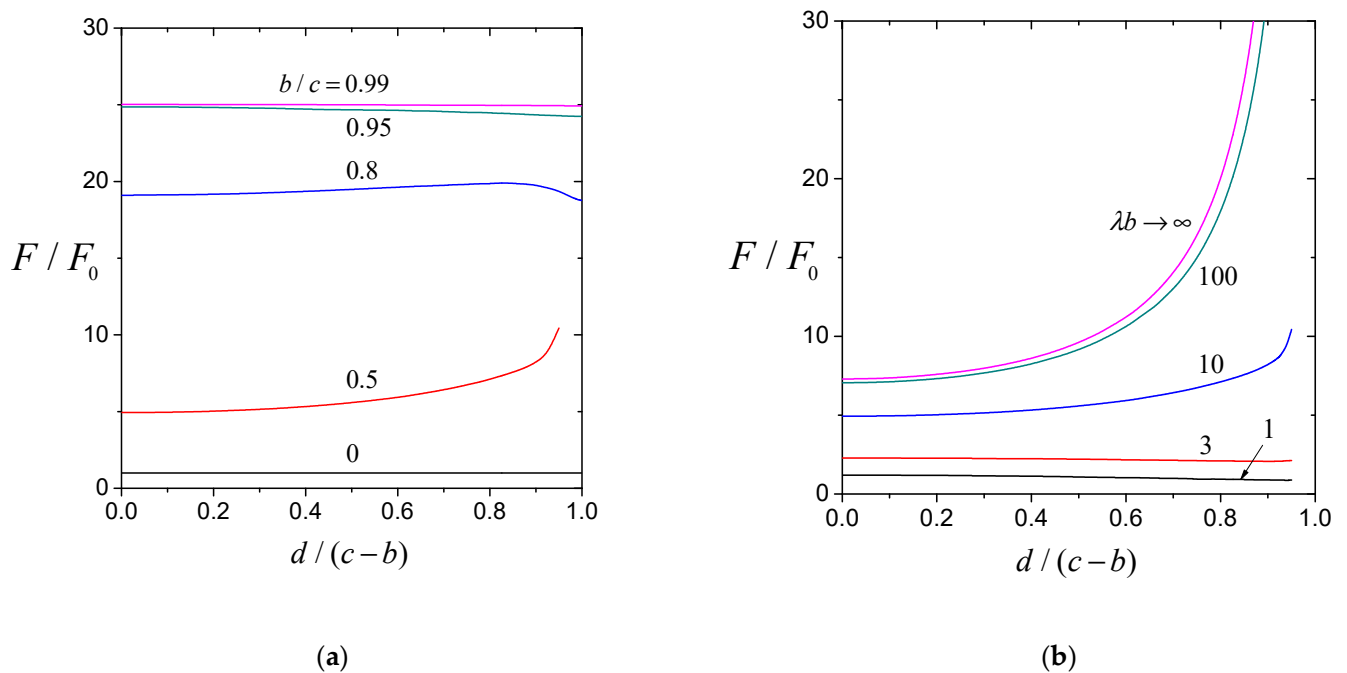
Figure 3. Normalized drag force F/F_0 of a porous sphere ($a = 0$) translating inside a spherical cavity versus the eccentricity parameter $d/(c-b)$: (**a**) $\lambda b = 10$ and (**b**) $b/c = 1/2$.

(a)

(b)
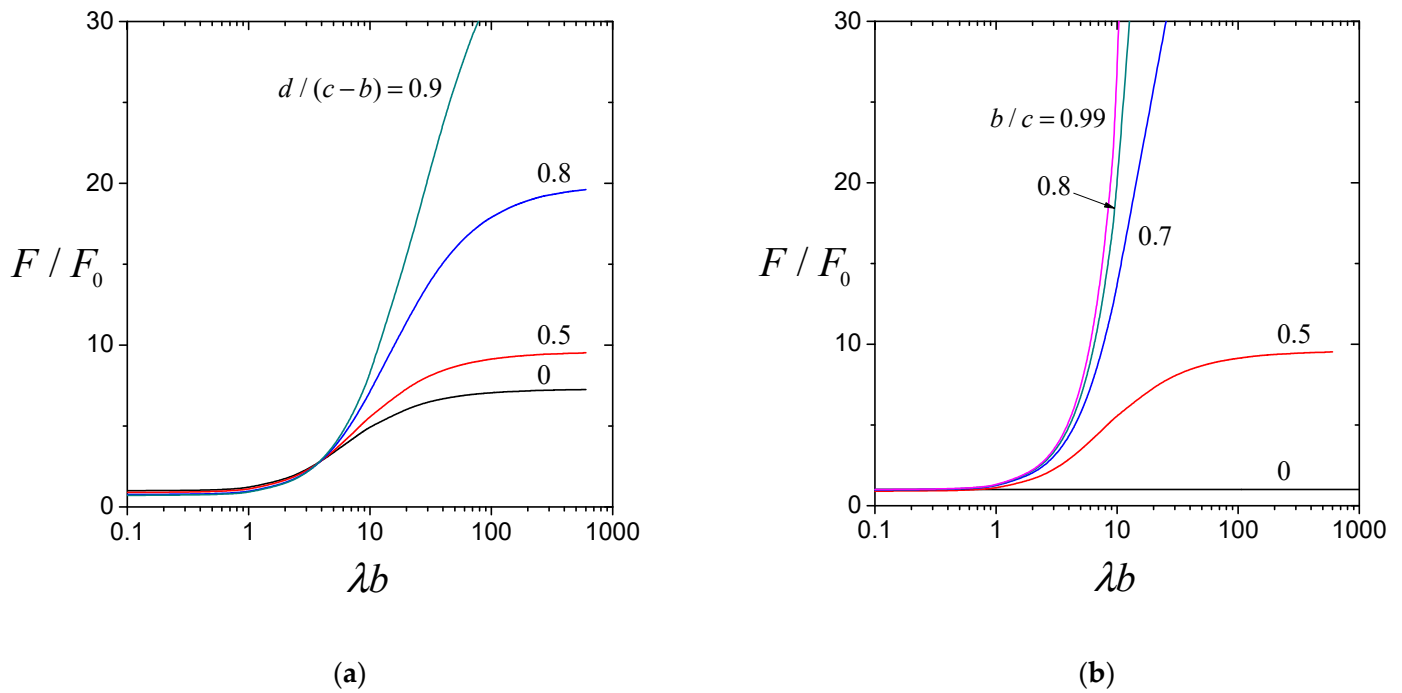
Figure 4. Normalized drag force F/F_0 of a porous sphere ($a = 0$) translating inside a spherical cavity versus the shielding parameter λb: (**a**) $b/c = 1/2$ and (**b**) $d/(c - b) = 1/2$.

Having realized the hydrodynamic effects of the non-concentric cavity on a translating porous particle, we can examine the general case of a translating soft particle. In Figures 5–8 and Table 2, the normalized force F/F_0 on a soft spherical particle within the cavity is shown as functions of the particle-to-cavity radius ratio b/c, core-to-particle radius ratio a/b, shielding parameter λb, and eccentricity parameter $d/(c - b)$, respectively. Likewise, F/F_0 is a monotonically increasing function of λb from a constant at $\lambda b = 0$ to a finite value (or infinity at the limit $b/c = 1$) as $\lambda b \to \infty$, generally increases with b/c from unity at $b/c = 0$ to a finite value (or infinity in the limit $\lambda b \to \infty$) at $b/c = 1$, and generally rises with increasing $d/(c - b)$ from one finite value in the concentric situation $d/(c - b) = 0$ to another at the contact limit $d/(c - b) = 1$, keeping the other parameters unchanged. When the value of a/b is small, $d/(c - b)$ is not near zero, and λb is smaller than about two, F/F_0 may first decrease as b/c increases from unity at $b/c = 0$, reach a minimum with $F/F_0 < 1$, and then rise with the further increase in b/c up to a value larger than unity at $b/c = 1$, as shown in Figure 6 and Table 2. In addition, when the values of λb and a/b are small (such as less than 3 and 0.5, respectively), F/F_0 may decrease slightly (even to less than unity) as $d/(c - b)$ increases, as illustrated in Table 2 and Figures 5, 7, and 8.

For fixed values of λb, $d/(c - b)$ and b/c, Figures 5–8 and Table 2 show that the normalized force F/F_0 on a translating soft sphere within a spherical cavity monotonically increases with a rise in the ratio of core-to-particle radii a/b, in which the cases of $a/b = 0$ and $a/b = 1$ denote the porous particle (the hard core disappears) and solid particle (the porous surface layer vanishes), respectively. That is, for given values of the particle radius, permeability of the porous layer, and separation from the wall (λb, $d/(c - b)$, and b/c), the force acting on the particle becomes less if the porous surface layer is thicker (a/b is smaller). All force results of the soft particle fall between the upper and lower bounds of $a/b = 1$ and $a/b = 0$, respectively. When the porous layer of the soft particle has small to moderate permeability (say. $\lambda b \geq 10$), F/F_0 on the soft particle with a/b being less than about 0.8 within a spherical cavity can be well approximated by the normalized force on a porous particle having identical permeability, radius, and eccentricity inside an identical cavity, as illustrated in Figures 5b and 8. Here, the hard core of the soft sphere barely feels the

relative motion of the fluid and exerts only negligible hindrance. But, this approximation does not apply to surface layers with high permeability.
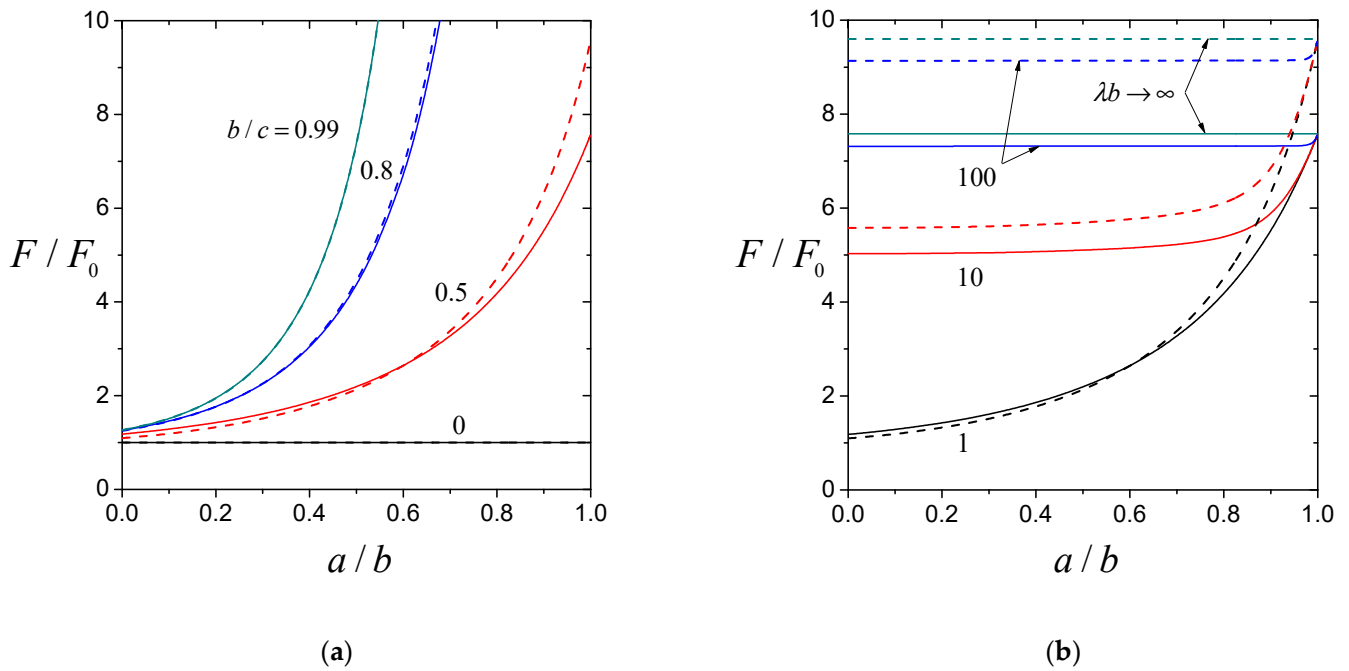

(**a**)

(**b**)

Figure 5. Normalized drag force F/F_0 of a soft spherical particle translating inside a spherical cavity versus the ratio of core-to-particle radii a/b: (**a**) $\lambda b = 1$ and (**b**) $b/c = 1/2$. The solid and dashed curves denote $d/(c-b) = 1/5$ and $d/(c-b) = 1/2$, respectively.
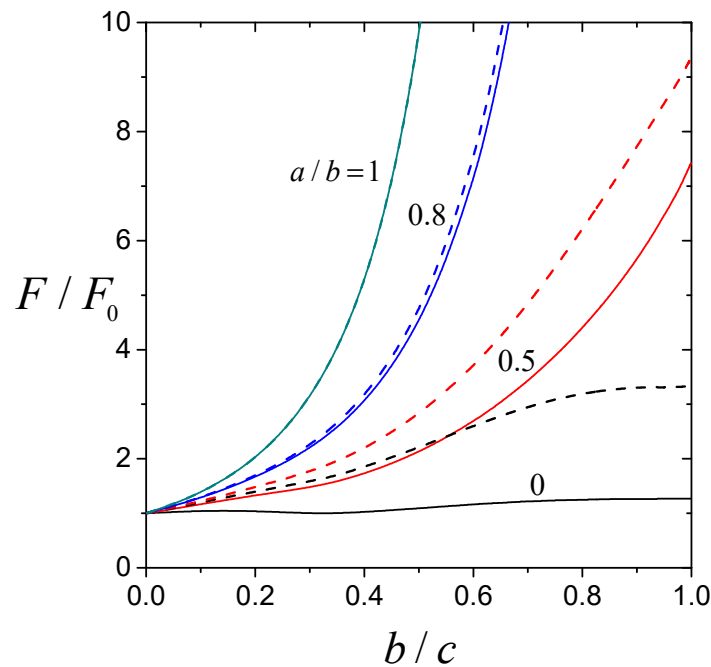

Figure 6. Normalized drag force F/F_0 of a soft sphere translating inside a spherical cavity with $d/(c-b) = 1/2$ versus the ratio of core-to-particle radii b/c. The solid and dashed curves denote $\lambda b = 1$ and $\lambda b = 3$, respectively.
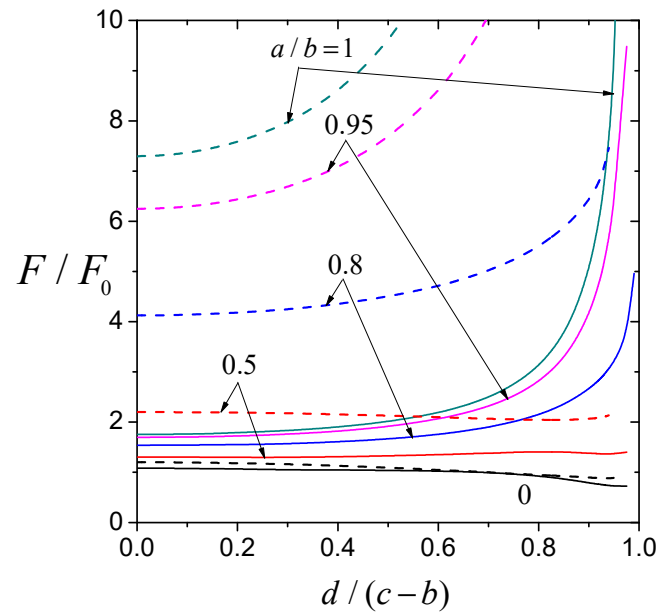
Figure 7. Normalized drag force F/F_0 of a soft sphere translating inside a spherical cavity with $\lambda b = 1$ versus the eccentricity parameter $d/(c-b)$. The solid and dashed curves denote $b/c = 1/5$ and $b/c = 1/2$, respectively.
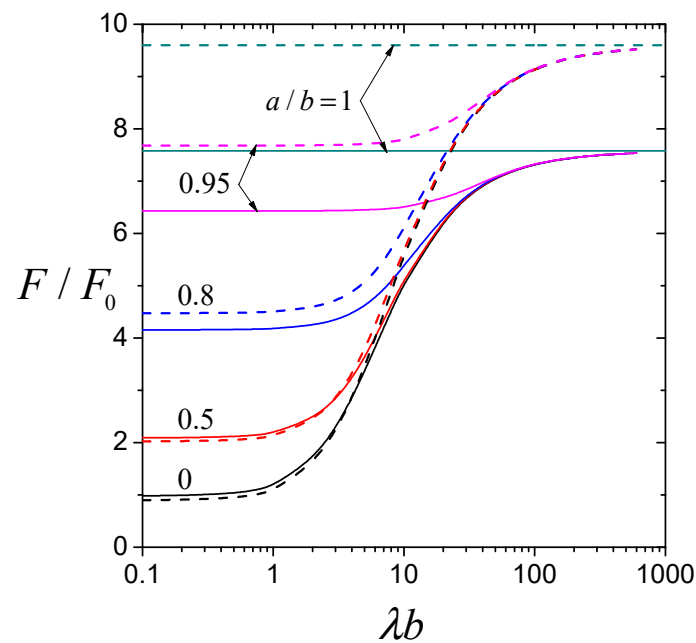
Figure 8. Normalized drag force F/F_0 of a soft sphere translating inside a spherical cavity with $b/c = 1/2$ versus the shielding parameter λb. The solid and dashed curves denote $d/(c-b) = 1/5$ and $d/(c-b) = 1/2$, respectively.

4. Concluding Remarks

The axially symmetric translation of a soft sphere in a viscous fluid within an eccentric spherical cavity is semi-analytically investigated in the quasi-steady limit of a small Reynolds number. A boundary collocation method is used to solve the Brinkman and Stokes equations for the fluid flows inside and outside the porous surface layer of the soft particle, respectively. Numerical results with good convergence for the normalized drag force F/F_0 exerted by the fluid on the particle are obtained for numerous values of the core-to-particle radius ratio a/b, particle-to-cavity radius ratio b/c, ratio of distance between the centers to radius difference of the particle and cavity $d/(c-b)$, and ratio of

particle radius to porous layer permeation length λb. The cavity wall effect on the drag force of a translating soft sphere includes monotonically increasing functions of a/b and λb. While F/F_0 generally increases with an increase in b/c, a weak minimum (surprisingly, smaller than unity) may occur for the case of low a/b and low λb. This normalized drag force generally increases with an increase in $d/(c - b)$, but for the case of low a/b and low λb, the drag force may decrease slightly with an increase in $d/(c - b)$.

We presented in Section 3 the solutions for a resistance problem, in which the drag force F acting on the soft sphere undergoing translation inside a spherical cavity is determined for a given particle velocity U. On the other hand, in a mobility problem, an applied force F acting on the particle is given and the wall-corrected particle velocity U needs to be determined. For the low-Reynolds-number translational motion of a soft sphere inside a cavity along their common diameter considered here, the normalized particle velocity U/U_0 [where U_0 is given by U in Equation (18) with $F_0 = F$] for a mobility problem is equal to the reciprocal normalized drag force, $(F/F_0)^{-1}$, provided by Tables 1 and 2 and Figures 2–8 for its matching resistance problem.

Appendix A

Some functions in Equations (11)–(15) are defined here.

$$A'_n(r,\theta) = -r^{n-2}[(n+1)G_{n+1}^{-1/2}(\cos\theta)\csc\theta - (2n-1)G_n^{-1/2}(\cos\theta)\cot\theta], \quad \text{(A1)}$$

$$A''_n(r,\theta) = -r^{n-2}[(2n-1)G_n^{-1/2}(\cos\theta) + P_n(\cos\theta)], \quad \text{(A2)}$$

$$B'_n(r,\theta) = -(n+1)r^{-n-1}G_{n+1}^{-1/2}(\cos\theta)\csc\theta, \quad \text{(A3)}$$

$$B''_n(r,\theta) = -r^{-n-1}P_n(\cos\theta), \quad \text{(A4)}$$

$$C'_n(r,\theta) = -r^n[(n+1)G_{n+1}^{-1/2}(\cos\theta)\csc\theta - (2n+1)G_n^{-1/2}(\cos\theta)\cot\theta], \quad \text{(A5)}$$

$$C''_n(r,\theta) = -r^n[(2n+1)G_n^{-1/2}(\cos\theta) + P_n(\cos\theta)], \quad \text{(A6)}$$

$$D'_n(r,\theta) = -r^{-n+1}[(n+1)G_{n+1}^{-1/2}(\cos\theta)\csc\theta - 2G_n^{-1/2}(\cos\theta)\cot\theta], \quad \text{(A7)}$$

$$D''_n(r,\theta) = -r^{-n+1}[2G_n^{-1/2}(\cos\theta) + P_n(\cos\theta)], \quad \text{(A8)}$$

$$\gamma'_n(r,\theta) = \lambda^{1/2}r^{-3/2}[\lambda r I_{-3/2}(\lambda r)G_n^{-1/2}(\cos\theta)\cot\theta - (n+1)I_{-1/2}(\lambda r)G_{n+1}^{-1/2}(\cos\theta)\csc\theta], \quad \text{(A9)}$$

$$\gamma''_n(r,\theta) = -\lambda^{1/2}r^{-3/2}[\lambda r I_{-3/2}(\lambda r)G_n^{-1/2}(\cos\theta) + I_{-1/2}(\lambda r)P_n(\cos\theta)], \quad \text{(A10)}$$

$$\delta'_n(r,\theta) = \lambda^{1/2}r^{-3/2}\{K_{n-1/2}(\lambda r)[nG_n^{-1/2}(\cos\theta)\cot\theta - P_{n-1}(\cos\theta)\sin\theta] - \lambda r K_{n+1/2}(\lambda r)G_n^{-1/2}(\cos\theta)\cot\theta\}, \quad \text{(A11)}$$

$$\delta''_n(r,\theta) = -\lambda^{1/2}r^{-3/2}\{K_{n-1/2}(\lambda r)[nG_n^{-1/2}(\cos\theta) + P_{n-1}(\cos\theta)\cos\theta] - \lambda r K_{n+1/2}(\lambda r)G_n^{-1/2}(\cos\theta)\}, \quad \text{(A12)}$$

$$A^*_n(r,\theta) = 2n(n-2)r^{n-3}G_n^{-1/2}(\cos\theta)\csc\theta, \quad \text{(A13)}$$

$$A_{1n}^{**}(r,\theta) = (-2n + 4 - \frac{\lambda^2 r^2}{n-1})r^{n-3}P_{n-1}(\cos\theta),\tag{A14}$$

$$A_{2n}^{**}(r,\theta) = -2(n-2)r^{n-3}P_{n-1}(\cos\theta),\tag{A15}$$

$$B_n^*(r,\theta) = 2(n^2-1)r^{-n-2}G_n^{-1/2}(\cos\theta)\csc\theta,\tag{A16}$$

$$B_{1n}^{**}(r,\theta) = (2n + 2 + \frac{\lambda^2 r^2}{n})r^{-n-2}P_{n-1}(\cos\theta),\tag{A17}$$

$$B_{2n}^{**}(r,\theta) = 2(n+1)r^{-n-2}P_{n-1}(\cos\theta),\tag{A18}$$

$$C_n^*(r,\theta) = 2(n^2-1)r^{n-1}G_n^{-1/2}(\cos\theta)\csc\theta,\tag{A19}$$

$$C_n^{**}(r,\theta) = -2(n-2-\frac{3}{n-1})r^{n-1}P_{n-1}(\cos\theta),\tag{A20}$$

$$D_n^*(r,\theta) = 2n(n-2)r^{-n}G_n^{-1/2}(\cos\theta)\csc\theta,\tag{A21}$$

$$D_n^{**}(r,\theta) = 2(n+1-\frac{3}{n})r^{-n}P_{n-1}(\cos\theta),\tag{A22}$$

$$\gamma_n^*(r,\theta) = -\lambda^{1/2}r^{-5/2}[2\lambda r I_{n+1/2}(\lambda r) - (2n^2-4n+\lambda^2 r^2)I_{n-1/2}(\lambda r)]G_n^{-1/2}(\cos\theta)\csc\theta,\tag{A23}$$

$$\gamma_n^{**}(r,\theta) = -2\lambda^{1/2}r^{-5/2}[\lambda r I_{n+1/2}(\lambda r) + (n-2)I_{n-1/2}(\lambda r)]P_{n-1}(\cos\theta),\tag{A24}$$

$$\delta_n^*(r,\theta) = \lambda^{1/2}r^{-5/2}[2\lambda r K_{n+1/2}(\lambda r) + (2n^2-4n+\lambda^2 r^2)K_{n-1/2}(\lambda r)]G_n^{-1/2}(\cos\theta)\csc\theta,\tag{A25}$$

$$\delta_n^{**}(r,\theta) = 2\lambda^{1/2}r^{-5/2}[\lambda r K_{n+1/2}(\lambda r) - (n-2)K_{n-1/2}(\lambda r)]P_{n-1}(\cos\theta),\tag{A26}$$

$$A_n^{***}(r,\theta) = -r^{n-2}[(n+1)G_{n+1}^{-1/2}(\cos\theta)\sec\theta + P_n(\cos\theta)],\tag{A27}$$

$$B_n^{***}(r,\theta) = B_n''(r,\theta) + B_n'(r,\theta)\tan\theta_2,\tag{A28}$$

$$C_n^{***}(r,\theta) = -r^n[(n+1)G_{n+1}^{-1/2}(\cos\theta)\sec\theta + P_n(\cos\theta)],\tag{A29}$$

$$D_n^{***}(r,\theta) = D_n''(r,\theta) + D_n'(r,\theta)\tan\theta_2,\tag{A30}$$

$$A_n^{****}(r,\theta) = -r^{n-2}[(2n-1)G_n^{-1/2}(\cos\theta)\csc^2\theta - (n+1)G_{n+1}^{-1/2}(\cos\theta)\csc\theta\cot\theta + P_n(\cos\theta)],\tag{A31}$$

$$B_n^{****}(r,\theta) = B_n''(r,\theta) - B_n'(r,\theta)\cot\theta_2,\tag{A32}$$

$$C_n^{****}(r,\theta) = -r^n[(2n+1)G_n^{-1/2}(\cos\theta)\csc^2\theta - (n+1)G_{n+1}^{-1/2}(\cos\theta)\csc\theta\cot\theta + P_n(\cos\theta)],\tag{A33}$$

$$D_n^{****}(r,\theta) = D_n''(r,\theta) - D_n'(r,\theta)\cot\theta_2,\tag{A34}$$

where P_n is the Legendre polynomial of order n.

Appendix B

For the slow translation of a soft sphere inside a concentric spherical cavity ($d = 0$), the exact solution of its drag force in Equation (17) was obtained explicitly as follows [19]:

$$D_{22} = 6\frac{U\gamma}{\lambda\Delta}[60\alpha\beta^2 - (2\beta^4 s_5 - 3\alpha^2 s_6 + \alpha\beta s_0 s_7)\cosh(\beta-\alpha)$$

$$+ (2\beta^3 s_8 + \alpha s_0 s_6 - 3\alpha^2\beta s_7)\sinh(\beta-\alpha)]\tag{A35}$$

where

$$\Delta = 12\alpha s_{22} + (9\alpha^2 s_{19} - \alpha s_0 s_{20} - 2\beta s_{21})\cosh(\beta-\alpha)$$

$$+ 3(2s_{23} + \alpha s_0 s_{19} - \alpha^2 s_{20})\sinh(\beta-\alpha),\tag{A36}$$

$$s_0 = \alpha^2 + 3, \quad s_5 = \beta^5 + 15\beta^3 - \gamma^5, \quad s_6 = 6\beta^5 + 45\beta^3 - \gamma^5,$$

$$s_7 = \beta^5 + 45\beta^3 - \gamma^5, \quad s_8 = 6\beta^5 + 15\beta^3 - \gamma^5,$$

$$s_{19} = 8\beta^5 - 15\beta^4\gamma + 60\beta^3 + 10\beta^2\gamma^3 - 3\gamma^5,$$

$$s_{20} = 4\beta^6 - 9\beta^5\gamma + 180\beta^4 + 10\beta^3\gamma(\gamma^2 - 18) - 9\beta\gamma^5 + 4\gamma^6,$$

$$s_{21} = 4\beta^8 - 9\beta^7\gamma + 60\beta^6 + 2\beta^5\gamma(5\gamma^2 - 63) - 3\beta^3\gamma(3\gamma^4 - 20\gamma^2 + 90) + 4\beta^2\gamma^6 + 6\gamma^6,$$

$$s_{22} = 20\beta^6 - 27\beta^5\gamma + 5\beta^3\gamma(\gamma^2 - 18) + 2\gamma^6,$$

$$s_{23} = 8\beta^8 - 15\beta^7\gamma + 20\beta^6 + 2\beta^5\gamma(5\gamma^2 - 36) - \beta^3\gamma(3\gamma^4 - 20\gamma^2 + 90) + 2\gamma^6, \quad \text{(A37)}$$

$$\alpha = \lambda a, \ \beta = \lambda b, \text{ and } \gamma = \lambda c.$$

References

1. Stokes, G.G. On the effect of the internal friction of fluids on the motion of pendulums. *Trans. Camb. Phil. Soc.* **1851**, *9*, 8–106.
2. Masliyah, J.H.; Neale, G.; Malysa, K.; van de Ven, T.G.M. Creeping flow over a composite sphere: Solid core with porous shell. *Chem. Eng. Sci.* **1987**, *42*, 245–253. [CrossRef]
3. Wunderlich, R.W. The effects of surface structure on the electrophoretic mobilities of large particles. *J. Colloid Interface Sci.* **1982**, *88*, 385–397. [CrossRef]
4. Anderson, J.L.; Solomentsev, Y. Hydrodynamic effects of surface layer on colloidal particles. *Chem. Eng. Comm.* **1996**, *148–150*, 291–314. [CrossRef]
5. Napper, D.H. *Polymeric Stabilization of Colloidal Dispersions*; Academic Press: London, UK, 1983.
6. Keh, H.J.; Chang, J.H. Boundary effects on the creeping-flow and thermophoretic motions of an aerosol particle in a spherical cavity. *Chem. Eng. Sci.* **1998**, *53*, 2365–2377. [CrossRef]
7. Keh, H.J.; Lee, T.C. Axisymmetric creeping motion of a slip spherical particle in a nonconcentric spherical cavity. *Theor. Comput. Fluid Dyn.* **2010**, *24*, 497–510. [CrossRef]
8. Lee, T.C.; Keh, H.J. Slow motion of a spherical particle in a spherical cavity with slip surfaces. *Int. J. Eng. Sci.* **2013**, *69*, 1–15. [CrossRef]
9. Alotaibi, M.A.; El-Sapa, S. Hydrophobic effects on a solid sphere translating in a Brinkman couple stress fluid covered by a concentric spherical cavity. *Phys. Fluids* **2024**, *36*, 033113. [CrossRef]
10. Brenner, H. The slow motion of a sphere through a viscous fluid towards a plane surface. *Chem. Eng. Sci.* **1961**, *16*, 242–251. [CrossRef]
11. Goldman, A.J.; Cox, R.G.; Brenner, H. Slow viscous motion of a sphere parallel to a plane wall—I. Motion through a quiescent fluid. *Chem. Eng. Sci.* **1967**, *22*, 637–651. [CrossRef]
12. Ganatos, P.; Weinbaum, S.; Pfeffer, R. A strong interaction theory for the creeping motion of a sphere between plane parallel boundaries. Part 1. perpendicular motion. *J. Fluid Mech.* **1980**, *99*, 739–753. [CrossRef]
13. Ganatos, P.; Pfeffer, R.; Weinbaum, S. A strong interaction theory for the creeping motion of a sphere between plane parallel boundaries. Part 2. Parallel motion. *J. Fluid Mech.* **1980**, *99*, 755–783. [CrossRef]
14. Chen, P.Y.; Keh, H.J. Slow motion of a slip spherical particle parallel to one or two plane walls. *J. Chin. Inst. Chem. Eng.* **2003**, *34*, 123–133.
15. Chang, Y.C.; Keh, H.J. Slow motion of a slip spherical particle perpendicular to two plane walls. *J. Fluids Struct.* **2006**, *22*, 647–661. [CrossRef]
16. Bungay, P.M.; Brenner, H. The motion of a closely-fitting sphere in a fluid-filled tube. *Int. J. Multiph. Flow* **1973**, *1*, 25–56. [CrossRef]
17. Leichtberg, S.; Pfeffer, R.; Weinbaum, S. Stokes flow past finite coaxial clusters of spheres in a circular cylinder. *Int. J. Multiph. Flow* **1976**, *3*, 147–169. [CrossRef]
18. Keh, H.J.; Chang, Y.C. Creeping motion of a slip spherical particle in a circular cylindrical pore. *Int. J. Multiph. Flow* **2007**, *33*, 726–741. [CrossRef]
19. Keh, H.J.; Chou, J. Creeping motion of a composite sphere in a concentric spherical cavity. *Chem. Eng. Sci.* **2004**, *59*, 407–415. [CrossRef]
20. Srinivasacharya, D.; Krishna Prasad, M. Steady rotation of a composite sphere in a concentric spherical cavity. *Acta Mech. Sin.* **2012**, *28*, 653–658. [CrossRef]
21. Prakash, J.; Raja Sekhar, G.P. Slow motion of a porous spherical particle with a rigid core in a spherical fluid cavity. *Meccanica* **2017**, *52*, 91–105. [CrossRef]
22. Prakash, J. Hydrodynamic mobility of a porous spherical particle with variable permeability in a spherical cavity. *Microsyst. Technol.* **2020**, *26*, 2601–2614. [CrossRef]
23. Chen, S.B.; Ye, X. Boundary effect on slow motion of a composite sphere perpendicular to two parallel impermeable plates. *Chem. Eng. Sci.* **2000**, *55*, 2441–2453. [CrossRef]
24. Jhuang, L.J.; Keh, H.J. Slow axisymmetric rotation of a soft sphere in a circular cylinder. *Eur. J. Mech. B Fluids* **2022**, *95*, 205–211. [CrossRef]
25. Faltas, M.S.; Saad, E.I. Slow Motion of a Porous Eccentric Spherical Particle-in-Cell Models. *Transp. Porous Med.* **2012**, *95*, 133–150. [CrossRef]

26. Saad, E.I. Axisymmetric motion of a porous sphere through a spherical envelope subject to a stress jump condition. *Meccanica* **2016**, *51*, 799–817. [CrossRef]

27. Sherief, H.H.; Faltas, M.S.; Saad, E.I. Stokes resistance of a porous spherical particle in a spherical cavity. *Acta Mech.* **2016**, *227*, 1075–1093. [CrossRef]

28. Koplik, J.; Levine, H.; Zee, A. Viscosity renormalization in the Brinkman equation. *Phys. Fluids* **1983**, *26*, 2864–2870. [CrossRef]

29. Chen, S.B. Axisymmetric motion of multiple composite spheres: Solid core with permeable shell, under creeping flow conditions. *Phys. Fluids* **1998**, *10*, 1550–1563. [CrossRef]

30. Neale, G.; Epstein, N.; Nader, W. Creeping flow relative to permeable spheres. *Chem. Eng. Sci.* **1973**, *28*, 1865–1874. [CrossRef]

31. Beavers, G.S.; Joseph, D.D. Boundary conditions at a naturally permeable wall. *J. Fluid Mech.* **1967**, *30*, 197–207. [CrossRef]